Microstructures and Electrochemical Properties of Rapidly-Solidified Si-Mn-Cr Alloy

Hyun Wook Han*, Deuk Kyu Ahn* Hyo-Jun Ahn**, Won Wook Park* and Keun Yong Sohn*

*School of Nano Engineering, Inje University,
607 O-bang dong, Gimhae, Gyeongnam 621-749, Republic of Korea, ksohn@inje.ac.kr
**School of Nano and Advanced Materials Engineering, Gyeongsang National University,
900 Gazwa-dong, Chinju, Gyeongnam 660-701, Republic of Korea, ahj@gnu.ac.kr

ABSTRACT

This paper presents the microstructures and electrochemical properties of Si-Mn-Cr alloy specimens prepared by a rapid solidification process and a conventional solidification process. $Si_{70}Mn_{15}Cr_{15}$ alloy specimens by atomic ratio were prepared by two different processes; arc-melting and melt spinning process. Results showed that the microstructures of $Si_{70}Mn_{15}Cr_{15}$ alloys consisted of Cr_4MnSi_{10} phase combined with a fine eutectic that is composed of silicon and Mn_4Si_7 phases. The volume fraction of Cr_4MnSi_{10} phase was over 0.8. The cycle efficiency of melt-spun ribbons was slightly improved compared to that of arc-melted ingot while the energy density was not dependent on the microstructural scale in this alloys. The energy density of arc-melted $Si_{70}Mn_{15}Cr_{15}$ alloy was significantly improved compared to the arc-melted binary $Si_{70}Mn_{30}$ alloys. The ternary phase, Cr_4MnSi_{10} compound appear to allow good cycle efficiency.

Keywords: melt-spinning, Si-Mn-Cr alloy, microstructure, electrochemical property

1 INTRODUCTION

Recently, Lithium-ion batteries of carbon based anode have been widely used because of their good electrochemical stability, long cycle life, fast charge-discharge rates combined with relatively high energy density. Although these carbon-based materials have excellent performance, since its theoretical capacity is $372mAhg^{-1}$[1-3], there is a limit to accommodate new-type portable devices which need much higher energy density. Many studies have been conducted to develop new anode materials that have higher specific capacity. Among alternative materials, silicon-based materials are one of the most attractive materials for lithium-ion batteries because silicon has a high theoretical specific capacity of about $4200mAhg^{-1}$[4-5]. However, silicon-based anode materials show rapid loss in capacity due to the mechanical failure of active materials caused by a large volume change during lithium insertion and extraction. Several works have been conducted to overcome the rapid degradation in the capacity and cycling efficiency. One effective way to improve the performance was decreasing the particle size of silicon [6-7]. Si-Mn and Si-Cr binary alloys showed a possibility to be used for secondary battery. Thin film Si-Mn [8] and Si-Cr [9] negative electrode materials produced by sputtering and annealing showed a relatively high energy capacity. The second discharge capacity of $Si_{70}Mn_{30}$ sputtered alloy by atomic ratio was reported to be about $1000mAhg^{-1}$[8]. In our previous work, the rapidly-solidified near-eutectic Si-Mn alloy ribbons showed greater energy density compared to the conventionally-solidified specimen [10].

The objective of this work is to investigate the microstructural change of Si-Mn alloy by the addition of Cr and to identify the effect of the phase change on the electrochemical behavior of the materials. In addition, the effects of microstructural scale on the electrochemical behavior of Si-Mn-Cr alloy are investigated by employing different solidification processes.

2 EXPERIMENTAL PROCEDURE

$Si_{70}Mn_{15}Cr_{15}$ alloy specimens by atomic ratio were prepared from high purity silicon (99.999%), commercial grade pure manganese (99.8%) and chromium (99.3%) by two different processes; arc-melting and arc-melting followed by melt spinning process. Conventionally-solidified specimens were prepared by arc-melting process, which was conducted under an argon atmosphere to produce a button shape of ingots of ~5g. In order to prepare rapidly-solidified ribbons, the raw materials were pre-alloyed by arc melting under an argon atmosphere. The pre-alloyed ingots were melt-spun to produce rapidly-solidified ribbons, for which the ingots were induction melted in a cylindrical graphite tube and ejected through a small orifice with 0.3mm in diameter using argon gas at a pressure of $0.4kgf/cm^2$. The ejected liquid jet impinges on a copper wheel rotating at 2,200 rpm to produce ~1mm wide and 20μm thick ribbons. The ribbons and arc-melted ingots were fragmented by mortar milling to produce a powder that could be passed through a 270-mesh sieve. Subsequently, acetylene black (AB), polyvinylidene fluoride (PVDF) and N-methylpyrrolidone (NMP, 5cc) were added into the alloy powder and mixed by planetary milling for 2 h. The mass ratio of the alloy powder, AB and PVDF was 2:4:4. The slurry was spread on a copper foil to prepare electrodes, which were dried in a vacuum chamber at room temperature for 24 h. A cell assembly was carried out under an argon atmosphere in a glove box, in which pure lithium was used as a counter electrode and Celgard 2400 film as a separator. $LiPF_6$

($1molL^{-1}$) dissolved in EC/DEC (1:1 volume ratio) was used as the electrolyte. The electrochemical properties of the cells were measured at $100mAg^{-1}$ current density between 0.01 and 2.0V using WBCS 3000 battery cycler. Microstructural evaluation and phase analysis were carried out by X-ray diffractometry (XRD), transmission electron microscopy (TEM) and scanning electron microscopy (SEM) combined with energy-dispersive spectrometry (EDS).

3 RESULTS AND DISCUSSION

3.1 Microstructures

The microstructures of melt-spun $Si_{70}Mn_{15}Cr_{15}$ ribbons mainly consist of Cr_4MnSi_{10} phase('C') combined with a fine eutectic that is composed of silicon ('A') and Mn_4Si_7('B') as shown in Fig. 1(a) and 1(b). Cr_4MnSi_{10} phase presented a spherical shape of ~500nm in diameter while silicon showed lamellar shape of 30~50nm thick. Fig. 1(b) is an enlarged view of Fig. 1(a). The EDS results acquired from the area marked as 'A', 'B' and 'C' in Fig. 1(b) were shown in Fig. 1(c), (d) and (e), respectively, indicating that "A" is silicon and "B" is a Si-Mn compound. Meanwhile, area 'C' was shown to be a Si-Mn-Cr ternary compound.

In the XRD patterns shown in Fig. 2, three phases were identified in the melt-spun $Si_{70}Mn_{15}Cr_{15}$ ribbons; α-Si, Mn_4Si_7 and Cr_4MnSi_{10}. Comparing with the XRD results of melt-spun $Si_{70}Mn_{30}$ ribbons [10], it can be identified that the intensity of diffraction peaks of α-Si and Mn_4Si_7 phases decreased significantly. Notably, the diffraction peaks corresponding to Cr_4MnSi_{10} phase were also observed. The phase was identified in the HRTEM image and diffraction patterns shown in Figure 1(e) as well. Thus, the area 'C' in Fig. 1(b) is confirmed as Cr_4MnSi_{10} phase. This result indicates that the microstructure of $Si_{70}Mn_{30}$ alloy changed to that with less volume fractions of α-Si and Mn_4Si_7 phases, while with a newly-formed Cr_4MnSi_{10} compound as the 50% of manganese atoms are replaced by chromium.

The arc-melted $Si_{70}Mn_{15}Cr_{15}$ ingot specimen showed relatively coarse microstructures as shown in Fig. 3, where Cr_4MnSi_{10} phase ('C') was shown to be as a continuous matrix. Silicon ('A') with thicknesses of 1~5 μm formed partially a eutectic with Mn_4Si_7('B') phase. Thus, melt spun ribbons showed ~50 fold smaller microstructural scales than those of arc-melted ingots.

In addition, there is a significant change in the relative volume fraction of each phase. In this ternary Si-Mn-Cr alloy, silicon formed a eutectic constituent with Mn_4Si_7 phase, similar to the microstructure shown in the binary $Si_{70}Mn_{30}$ alloy [10]. By the addition of chromium as a replacement of manganese, however, the volume fraction of silicon was significantly reduced (V_{Si}<0.1) while that of Cr_4MnSi_{10} phase significantly increased (V_{Si}<0.8) as shown in Fig. 3.

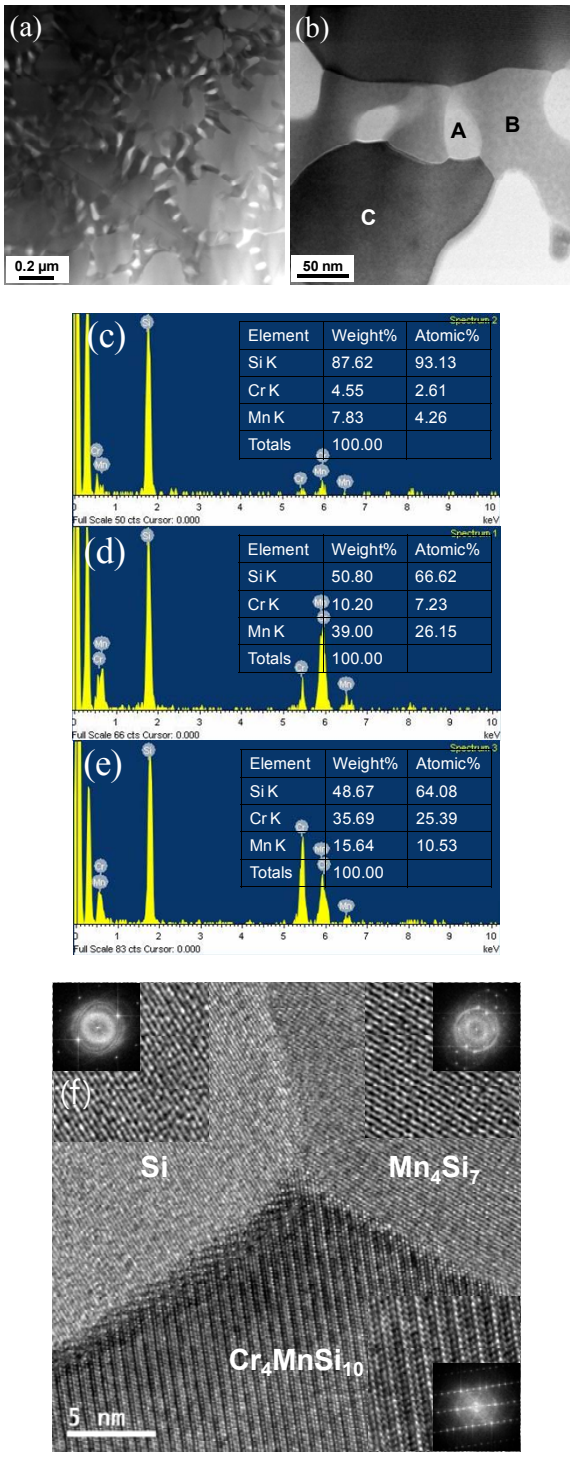

Figure 1: Microstructures of melt-spun $Si_{70}Mn_{15}Cr_{15}$ ribbons: (a) BFTEM; (b) Enlarged view of (a); (c) EDS of Area A of (b); (d) EDS of Area B of (b); (e) EDS of Area C of (b);(f) HRTEM of area (b).

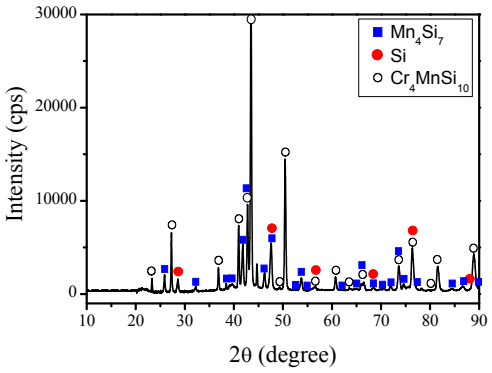

Figure 2: X-ray diffraction patterns of melt-spun $Si_{70}Mn_{15}Cr_{15}$ ribbons

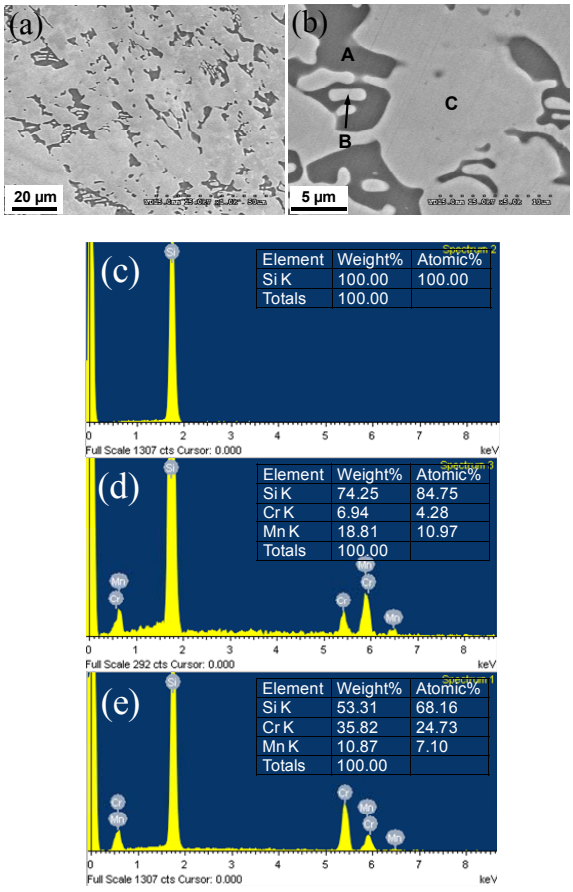

Figure 3: Microstructures of arc-melted $Si_{70}Mn_{15}Cr_{15}$ ingots: (a) SEM; (b) Enlarged view of (a); (c) EDS of Area A of (b); (d) EDS of Area B of (b); (e) EDS of Area C of (b).

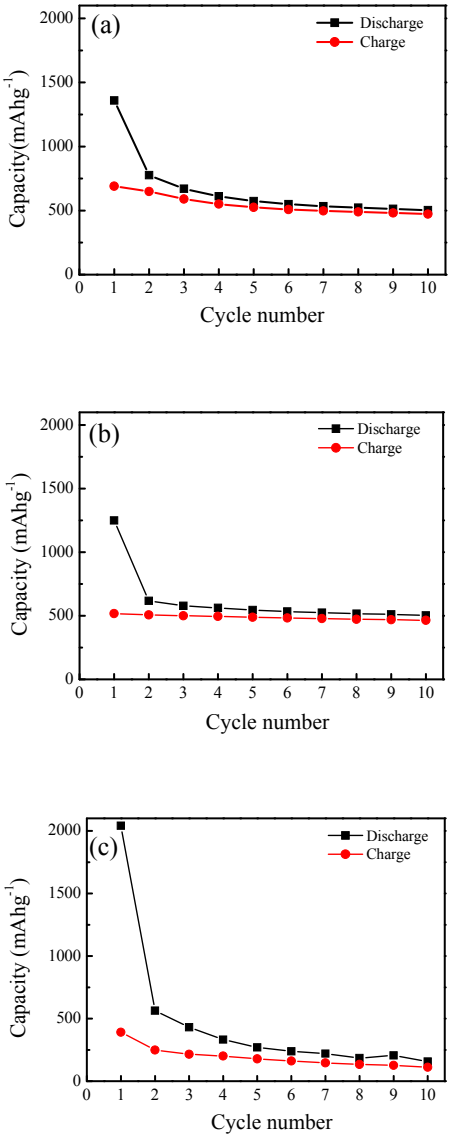

Figure 4: Variations of the specific capacity with the cycle number of (a) melt-spun ribbons and (b) arc-melted ingots of $Si_{70}Mn_{15}Cr_{15}$ alloy, and (c) arc-melted ingots of $Si_{70}Mn_{30}$ alloy.

3.2. Electrochemical Performance

The variations of specific capacity on the cycle number of the melt-spun $Si_{70}Mn_{15}Cr_{15}$ ribbons and the arc-melted $Si_{70}Mn_{15}Cr_{15}$ ingots were shown in Fig. 4. The first discharge capacity of melt-spun $Si_{70}Mn_{15}Cr_{15}$ ribbons was 1,249 $mAhg^{-1}$ while it gradually decreased to 502 $mAhg^{-1}$ after 10 cycles. The first discharge capacity of arc-melted specimen was 1,359 $mAhg^{-1}$, and it also gradually decreased to 502 $mAhg^{-1}$ after 10 cycles. The initial irreversible capacity of melt-spun ribbons

was 733 mAh^{-1}, while that of arc-melted ingot specimens was 669 mAh^{-1}.

The cycle performance of melt-spun $Si_{70}Mn_{15}Cr_{15}$ ribbons was slightly improved compared to that of arc-melted $Si_{70}Mn_{15}Cr_{15}$ ingot due to the fine microstructural scale. However, the energy density of the melt-spun ribbon did not significantly differ from that of arc-melted ingots, which is somewhat different from the data obtained from $Si_{70}Mn_{30}$ binary alloys as shown in Fig. 4(c). As mentioned before, the relative volume fraction of silicon the $Si_{70}Mn_{15}Cr_{15}$ ribbons was under 0.1, which is much smaller than that of the binary $Si_{70}Mn_{30}$ alloy with near-eutectic microstructures [10]. Thus, the energy density of the ternary alloy is expected to be significantly reduced. However, the difference was not so significant. The results reflect that the majority phase of the $Si_{70}Mn_{15}Cr_{15}$ ribbons, Cr_4MnSi_{10}, appears to involve in the intercalation reaction of lithium.

Fig. 5 shows cyclic voltamograms (CV), charge/discharge curves of melt-spun $Si_{70}Mn_{15}Cr_{15}$ ribbons and arc-melted ingots. Three reductive peaks can be seen, which correspond to the formation of the SEI film (0.6 V) and insertion of lithium into silicon. The other two reduction peaks and the oxidation peaks explain that capacity fade is much smaller than that of melt-spun $Si_{70}Mn_{30}$ ribbons by the addition of chromium. Meanwhile, plateau at 0.5V in charge/discharge curves of arc-melted $Si_{70}Mn_{15}Cr_{15}$ ingots gradually decreased.

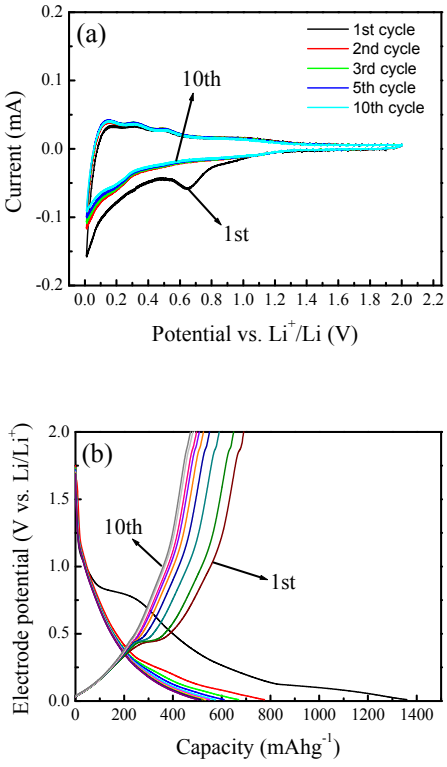

Figure 5: Cyclic voltammograms (a) and charge/discharge curves (b) of melt-spun ribbons.

The cycle stability of melt-spun $Si_{70}Mn_{15}Cr_{15}$ ribbons was somewhat improved compared to that of arc-melted ingot. The reason seemed to be the fine microstructural scale of melt-spun ribbons. As the size of silicon phase reduced, relatively large available surface area and small diffusion distance for lithium-ion exchange were obtained. The energy density of melt-spun $Si_{70}Mn_{15}Cr_{15}$ ribbons was similar to that of arc-melted ingots after 10 cycles. The reason for the similarity is the enhanced energy density for the arc-melted $Si_{70}Mn_{15}Cr_{15}$ ingots compared to the arc-melted $Si_{70}Mn_{30}$ ingots. It was identified that the majority phase in $Si_{70}Mn_{15}Cr_{15}$ alloy was Cr_4MnSi_{10} compound. Thus, the enhanced energy density of arc-melted $Si_{70}Mn_{15}Cr_{15}$ alloy represents that the Cr_4MnSi_{10} phase played an important role. The relatively low packing factor due to large lattice constants of Cr_4MnSi_{10} phase would be partly responsible for the reasons.

4 CONCLUSIONS

1. The microstructure of $Si_{70}Mn_{15}Cr_{15}$ alloy was composed of a eutectic constituent consisting of α-Si and Mn_4Si_7, and an intermetallic compound matrix, Cr_4MnSi_{10} phase. The volume fraction of Cr_4MnSi_{10} phase was over 0.8.
2. The cycle stability of melt-spun $Si_{70}Mn_{15}Cr_{15}$ ribbons was somewhat improved compared to that of arc-melted $Si_{70}Mn_{15}Cr_{15}$ ingot. However, energy density of melt-spun $Si_{70}Mn_{15}Cr_{15}$ ribbons was not significantly enhanced when compared to that of arc-melted ingots.
3. The energy density of arc-melted $Si_{70}Mn_{15}Cr_{15}$ alloy was significantly improved compared to the arc-melted binary $Si_{70}Mn_{30}$ alloys because of Cr_4MnSi_{10} phase, which allows good cycle efficiency.

REFERENCES

[1] C. Menachem, E. Peled, L. Burstein, Y. Rosenberg, J. Power Sources, 68, 277, 1997.
[2] T.D. Hatchard, M.N. Obrovac, J.R. Dahn, J. Electrochem. Soc. 152, A2335, 2005.
[3] A. Bonakdarpour, K.C. Hewitt, R.L. Turner, J.R. Dahn, J. Electrochem. Soc. 151, A470, 2004.
[4] M.N. Obrovac and L. Christensen, Electrochem. Solid-State Lett. 7, A93, 2004.
[5] T.D. Hatchard and J.R. Dahn, J. Electrochem. Soc. 151, A838, 2004.
[6] C.S. Wang, G.T. Wu, X.B. Zhang, Z.F. Qi, W.Z. Li, J. Electrochem. Soc. 145, A2751, 1998.
[7] H. Li, X. Huang, L. Chen, Z.Wu, Y. Liang, Electrochem. Solid State Lett. 2, 547, 1999.
[8] M.D. Fleischauer, J.M. Topple, J.R. Dahn, Electrochem. Solid-State Lett. 8, A137, 2005.
[9] W.J. Weydanz, M. Wohlfahrt-Mehrens, R.A. Huggins, J. Power Sources 81, 237, 1999.
[10] H.Y. Han, D.K. Ahn, H.-J. Ahn, W.-W. Park, K.Y. Sohn, Rev. Adv. Mater. 28, 14, 2011,.